PNAS
www.pnas.org

Supplementary Information for

# Phase separation and clustering of an ABC transporter in *Mycobacterium tuberculosis*

Florian Heinkel, Libin Abraham, Mary Ko, Joseph Chao, Horacio Bach, Loktin Hui, Haoran Li, Mang Zhu, Yeou Mei Ling, Jason Rogalski, Joshua Scurll, Jennifer M. Bui, Thibault Mayor Michael R. Gold, Keng C. Chou, Yossef Av-Gay, Lawrence P. McIntosh[1], Jörg Gsponer[1]

[1] Corresponding authors.

Email: gsponer@msl.ubc.ca (J.G.) and mcintosh@chem.ubc.ca (L.P.M.)

This PDF file includes:

## Supplementary Materials and Methods

### Expression and purification of Rv1747$^{1-310}$ for droplet studies

Using *M. tuberculosis* H37Rv genomic DNA as a template, the gene encoding the regulatory module (residues 1-310) of Rv1747 was PCR-amplified and cloned with a TAA stop codon into the pET28MHL plasmid (Addgene #26096) via *Nde*I and *Hind*III restriction sites. Codons for a single N-terminal cysteine for fluorescent labeling, as well as phospho-ablative threonine to alanine mutants (T152A/T210A) of the Rv1747$^{1-310}$ construct, were introduced via PCR-based and QuikChange (Stratagene) site-directed mutagenesis protocols, respectively. After cleavage of an N-terminal $His_6$-affinity tag with TEV protease, two non-native residues (Gly-His) proceeded the expressed Rv1747 fragments.

Proteins were expressed in *E. coli* Rosetta 2 (λDE3) cells in LB media supplemented with 35 μg/mL chloramphenicol and 35 μg/mL kanamycin. Cultures of 1 L were incubated shaking at 37 °C until $OD_{600}$ ~ 0.6, induced with IPTG (1 mM final) and grown for another 16 h at 24 °C. The cells were collected by centrifugation for 15 min at 4000 g, frozen at -80 °C, then later thawed, resuspended in lysis buffer (20 mM sodium phosphate, 1 M NaCl, 10 mM imidazole, pH 8.0) and sonicated. After centrifugation for 1 h at 30000 g, the supernatant was filtered (0.45 μm cutoff), applied to a $Ni^{2+}$-NTA HisTrap HP affinity column (GE Healthcare Life Sciences), washed with 10 column volumes of binding buffer (20 mM sodium phosphate, 500 mM NaCl, 30 mM imidazole, pH 8.0) and eluted in a 30 – 500 mM imidazole gradient. Fractions containing the desired protein were identified with SDS-PAGE, pooled and treated with $His_6$-tagged TEV protease while dialyzing against 4 L of cleavage buffer (20 mM sodium phosphate, 100 mM NaCl, 1 mM DTT, 0.5 mM EDTA, pH 7) for 16 h at 4 °C. Uncleaved protein, cleaved tag and TEV were

removed using a second $Ni^{2+}$-NTA HisTrap HP affinity purification step, and the collected flow-through was concentrated and subjected to size-exclusion chromatography using a Superdex 75 (GE Healthcare) column with sample buffer (100 mM NaCl, 20 mM sodium phosphate, pH 6.0). In the case of $Rv1747^{1-310}$ samples for studies on supported lipid bilayers (SLBs), cleavage with TEV protease was omitted and the concentrated fractions from the initial $Ni^{2+}$-NTA HisTrap purification were subjected to size-exclusion chromatography directly. Final protein fractions were pooled, concentrated using a 10 kDa MWCO centrifugal filter (EMD Millipore), flash frozen and stored at -80 °C. Samples were verified by SDS-PAGE and electrospray ionization mass spectrometry (ESI-MS), and their concentrations determined by UV-absorbance spectroscopy using the predicted molar absorptivity $\varepsilon_{280}$ of 24000 $M^{-1}$ $cm^{-1}$ (1).

**Expression and purification of MSMEG_$1642^{1-340}$ for droplet studies**

The gene encoding residues 1-340 of *M. smegmatis*, MSMEG_$1642^{1-340}$, codon-optimized for expression in *E. coli*, was purchased from Integrated DNA Technologies and cloned into the pET28MHL plasmid (Addgene #26096) via *Nde*I and *Hind*III restriction sites. Expression in *E. coli* Rosetta 2 (λDE3) cells and purification was done as for $Rv1747^{1-310}$ without cleavage of the $His_6$-tag. Protein concentration was determined using a predicted molar absorptivity $\varepsilon_{280}$ of 31000 $M^{-1}$ $cm^{-1}$ (1).

**Expression and purification of active kinase domain constructs of *Mtb* STPKs**

Genes encoding $PknA^{1-337}$, $PknD^{1-369}$, $PknE^{1-336}$, $PknF^{1-292}$, $PknJ^{1-343}$, $PknK^{1-299}$ and $PknL^{1-369}$ were cloned from *Mtb* H37Rv genomic DNA into the pGEX-4T3 plasmid (GE Healthcare) using *Bam*HI and *Xho*I restriction sites. A codon for an N-terminal cysteine, used for fluorophore

conjugation, was introduced into gene encoding $PknF^{1-292}$ via the QuikChange (Stratagene) site directed mutagenesis protocol. The resulting constructs, with an N-terminal glutathione S-transferase (GST) affinity tag, were expressed in *E. coli* BL21 (λDE3) cells in LB media supplemented with 100 μg/mL ampicillin. Cultures of 1 L were incubated at 37 °C until $OD_{600}$ ~ 0.6, induced with ITPG and grown as summarized in Table S1. After centrifugation for 15 min at 4000 g, the cell pellet from each given preparation was frozen at -80 °C, then later thawed, resuspended in lysis buffer (10 mM sodium phosphate, 1.8 mM potassium phosphate, 140 mM NaCl, 2.7 mM KCl, pH 7.3) and sonicated. The supernatant was centrifuged for 1 h at 30000 g, filtered, applied to a GSTrap HP affinity column (GE Healthcare), washed with 10 column volumes of the same buffer, and eluted with 50 mM Tris, 10 mM reduced glutathione at pH 7.4. After SDS-PAGE analysis, pooled fractions were subjected to size-exclusion chromatography using a Superdex 75 (GE Healthcare) column in storage buffer (100 mM NaCl, 20 mM sodium phosphate, pH 7.4). Final protein factions were pooled, concentrated using a 10 kDa MWCO centrifugal filter (EMD Millipore), flash frozen and stored at -80 °C. Samples were verified by SDS-PAGE and concentrations determined by UV-absorbance spectroscopy using predicted molar absorptivities $\varepsilon_{280}$ (Table S1) (1).

Genes encoding $PknB^{8-292}$, $PknG^{1-750}$ and $PknH^{1-399}$ were cloned into pET22b via *BamH*I and *Xho*I restriction sites. The constructs, with a C-terminal $His_6$-affinity tag for purification, were expressed in *E. coli* BL21 (λDE3) cells in LB media supplemented with 100 μg/mL ampicillin. Cultures of 1 L were incubated with shaking at 37 °C until $OD_{600}$ ~ 0.6, induced with IPTG and grown as summarized in Table S1. After centrifugation for 15 min at 4000 g, each cell pellet was frozen at -80 °C, then later thawed, resuspended in lysis buffer (20 mM sodium phosphate, 1 M NaCl, 10 mM imidazole, pH 8.0) and sonicated. After centrifugation for 1 h at 30000 g, the

supernatant was filtered (0.45 μm cutoff), applied to a $Ni^{2+}$-NTA HisTrap HP affinity column (GE Healthcare), washed with 10 column volumes of binding buffer (20 mM sodium phosphate, 500 mM NaCl, 30 mM imidazole, pH 8.0) and eluted in a 30 – 500 mM imidazole gradient. Fractions containing the desired protein were identified with SDS-PAGE, pooled, concentrated and subjected to size-exclusion chromatography using a Superdex 75 (GE Healthcare) column with sample buffer (100 mM NaCl, 20 mM sodium phosphate, pH 6.0). Final protein fractions were pooled, concentrated using a 10 kDa MWCO centrifugal filter (EMD Millipore), flash frozen and stored at -80 °C. Samples were verified by SDS-PAGE and concentrations determined by UV-absorbance spectroscopy using predicted molar absorptivities $\varepsilon_{280}$ (Table S1) (1).

**Table S1**. Expression conditions for STPK constructs

| Kinase | Amino Acids | Vector | Expression Temp./Time | IPTG [mM] | Predicted $\varepsilon_{280}$ ($M^{-1}$ $cm^{-1}$) |
|---|---|---|---|---|---|
| **PknA** | 1-337 | pGEX-4T3 | 22 °C, 16 hr | 0.5 mM | 59000 |
| **PknB** | 1-332 | pET22b | 22 °C, 16 hr | 0.5 mM | 15000 |
| **PknD** | 1-369 | pGEX-4T3 | 16 °C, 16 hr | 1 mM | 71000 |
| **PknE** | 1-336 | pGEX-4T3 | 22 °C, 16 hr | 0.5 mM | 76000 |
| **PknF** | 1-292 | pGEX-4T3 | 22 °C, 16 hr | 0.5 mM | 70000 |
| **PknG** | 1-750 | pET22b | 22 °C, 16 hr | 0.1 mM | 74000 |
| **PknH** | 1-399 | pET22b | 37 °C, 4 hr | 1 mM | 46000 |
| **PknJ** | 1-343 | pGEX-4T3 | 22 °C, 16 hr | 0.5 mM | 83000 |
| **PknK** | 1-299 | pGEX-4T3 | 22 °C, 16 hr | 0.5 mM | 56000 |
| **PknL** | 1-369 | pGEX-4T3 | 22 °C, 16 hr | 0.5 mM | 64000 |

**Expression of the PstP phosphatase domain**

The gene encoding $PstP^{1-240}$ was PCR amplified and cloned with a TAA stop codon into the pET28MHL plasmid (Addgene #26096) via *Nde*I and *Hind*III restriction sites. An N-terminal single cysteine was introduced for fluorescent labeling. The $His_6$-tagged protein was expressed in *E. coli* Rosetta 2 (λDE3) cells in LB media supplemented with 35 μg/mL chloramphenicol and 35 μg/mL kanamycin. Cultures of 1 L were incubated with shaking at 37 °C until $OD_{600}$ ~ 0.6, induced with IPTG (1 mM final) and grown for another 16 h at 24 °C. The cells were collected by centrifugation for 15 min at 4000 g, frozen at -80 °C, then later thawed, resuspended in lysis buffer (20 mM sodium phosphate, 1 M NaCl, 10 mM imidazole, pH 8.0) and sonicated. After centrifugation for 1 h at 30000 g, the supernatant was filtered (0.45 μm cutoff), applied to a $Ni^{2+}$-NTA HisTrap HP affinity column (GE Healthcare Life Sciences), washed with 10 column volumes of binding buffer (20 mM sodium phosphate, 500 mM NaCl, 30 mM imidazole, pH 8.0) and eluted in a 30 – 500 mM imidazole gradient. Fractions containing the desired protein were identified with SDS-PAGE, pooled, concentrated and subjected to size-exclusion chromatography using a Superdex 75 (GE Healthcare) column with sample buffer (100 mM NaCl, 20 mM sodium phosphate, pH 6.0). Final protein fractions were pooled, concentrated using a 10 kDa MWCO centrifugal filter (EMD Millipore), flash frozen and stored for further use at -80 °C. Samples were verified by SDS-PAGE and concentrations determined by UV-absorbance spectroscopy using $\varepsilon_{280}$ = 6100 $M^{-1}$ $cm^{-1}$ (1).

For simplicity, the constructs of catalytic domains of the STPKs and PstP are denoted without specifying the affinity tag and residue numbering.

**Fluorescent labeling of Rv1747$^{1-310}$, GST-PknF$^{1-292}$ and PstP$^{1-240}$**

Rv1747$^{1-310}$ with a non-native N-terminal cysteine was conjugated with Oregon Green (OG, Invitrogen). Using the same strategy of specific labelling via an introduced, N-terminal cysteine, GST-PknF$^{1-292}$ and His$_6$-PstP$^{1-240}$ were conjugated with Alexa Fluor 647 (AF647, Invitrogen). For the conjugation reactions, a 10-fold molar excess of maleimide-functionalized fluorescent dye was added to protein samples in conjugation buffer (100 mM NaCl, 20 mM sodium phosphate, 1 mM TCEP, pH 7.0) and incubated at 22 °C in the dark while constantly inverting for 120 min. The reactions were stopped by the addition of 1 mM of reduced glutathione. Samples were then subjected to size-exclusion chromatography using a Superdex 75 (GE Healthcare) column with sample buffer (100 mM NaCl, 20 mM sodium phosphate, pH 6.0). Final protein fractions were pooled, concentrated using a 10 kDa MWCO centrifugal filter (EMD Millipore), flash frozen and stored at -80 °C. Concentrations of protein samples were determined by UV-absorbance as stated above. Labeling efficiencies with the fluorescent dyes were 5 – 10 % as determined using UV-absorbance and the molar absorptivities at the maximum absorbance for OG and AF647 of $\varepsilon_{496}$ = 70000 $M^{-1}$ $cm^{-1}$ and $\varepsilon_{650}$ = 270000 $M^{-1}$ $cm^{-1}$, respectively.

**Phase separation of Rv1747$^{1-310}$ enhanced by *Mtb* STPK phosphorylation**

Phase separation depends on numerous factors such as protein concentration, incubation time with a kinase, and sample conditions including temperature. For consistency, we developed a standard protocol for all experiments performed in this study. Samples of OG-Rv1747$^{1-310}$ at the indicated concentrations were incubated at 22 °C for 120 min with different molar ratios of the PknF kinase domain in 20 mM sodium phosphate, 100 mM NaCl, and 5 mM $MgCl_2$ at pH 7.4. To ensure low level phosphorylation of 50 µM OG-Rv1747$^{1-310}$, the PknF:OG-Rv1747$^{1-310}$ molar ratio

was 1:100 and the ATP was 100 μM. For higher level phosphorylation, the ratio was 1:10 with 5 mM ATP. Reactions for microscopy were performed in CoverWell imaging chambers (Sigma-Aldrich) that were pre-treated with 30 mg/mL BSA for 30 min, rinsed with double-distilled $H_2O$ and dried before use. Phosphorylation levels after 120 min were determined by ESI-MS on thoroughly re-suspended samples of droplets.

**Phase separation of unmodified Rv1747$^{1-310}$**

Samples of OG-Rv1747$^{1-310}$ were slowly concentrated at 22 °C and 2000 g in 10 kDa MWCO centrifugal filters (EMD Millipore). Frequently, centrifugation was stopped, the sample thoroughly resuspended, and the concentration determined using UV-absorbance. Part of the resuspended sample was also transferred to pre-treated CoverWell imaging chambers (Sigma-Aldrich) and incubated for 120 min before fluorescent imaging and quantification of phase separation as described below.

**Dephosphorylation of Rv1747$^{1-310}$ by PstP and dissolution assay of droplets**

Phase separation was induced by addition of 0.5 μM PknF to samples of 50 μM OG-Rv1747$^{1-310}$ in 20 mM sodium phosphate, 100 mM NaCl, 100 μM ATP, 5 mM $MgCl_2$ and 5 mM $MnCl_2$ at pH 7.4. After 120 min, 5 μM PstP was added to one of two samples and droplets were monitored over 24 h at 22 ºC by confocal fluorescence microscopy.

**Radioactive γ-$^{32}$P kinase assay of *Mtb* STPKs on Rv1747$^{1-310}$**

Purified samples of 10 μM of Rv1747$^{1-310}$ and Rv1747$^{1-310}$ T152A/T210A were incubated with 5 μCi of [γ-$^{32}$P]ATP in a buffer containing 20 mM sodium phosphate, 100 mM NaCl, 1 mM

DTT, 5 mM $MgCl_2$ and 5 mM $MnCl_2$ and 0.5 – 2 μM of STPK kinase domain at pH 7.4. The incubation was performed at room temperature (~ 22 °C) for 5 to 10 min. The reactions were stopped with SDS-sample loading buffer and heated at 95 °C for 10 min. Samples were resolved by a 12 % SDS-PAGE. The gels were silver stained and dried. The $^{32}$P-radioactively labeled bands of phosphorylated protein were detected using a PhosphorImager SI (Molecular Dynamics).

**Phospho-acceptor site mapping by mass spectrometry**

Samples of Rv1747$^{1-310}$ (50 μM) were treated with PknF (5 μM kinase domain with 5 μM mM ATP and 5 mM $MgCl_2$ in buffer containing 20 mM sodium phosphate, 100 mM NaCl, pH 6) at room temperature. Aliquots were removed at several time points, flash frozen, and then assayed by ESI-MS for phosphorylation levels. After an initial 15 min of kinase treatment, the Rv1747$^{1-310}$ was a mixture of species modified with 1, 2 and 3 phosphates. After a final 60 min, this increased to a mixture with 3 and 4 phosphates, as well as a minor amounts with 2 and 5 phosphates. Following previously described methods (2), samples from these two time points were digested with trypsin and 10 pmol were loaded onto an capillary flow LC-MS/MS system (Agilent 6550 with Agilent 1260 HPLC). Peptides were subjected to collision induced dissociation MS/MS. The raw data were analysed with the Byonic (Protein Metrics Inc) database search algorithm against the UniProt *Mtb* proteome database. Peptide spectrum matches that were identified to contain a phosphorylated residue were manually validated. Although the overall phosphorylation levels increased with time, the same phospho-acceptor sites were identified in the two samples.

**Imaging of Rv1747$^{1-310}$ and MSMEG_1642$^{1-340}$ droplets**

Differential interference contrast (DIC) and fluorescence microscopy were performed on a Olympus FV1000 inverted confocal microscope with an UplanSApo 60× 1.35 numerical aperture

(NA) oil immersion objective. All images were acquired at ~ 22 °C (room temperature) while maintaining consistent lamp/laser power, exposure time, gain, and offset. For fluorescent images, excitation lasers generated 473 nm (OG) and 633 nm (AF647) wavelength light and emission filters for maxima at 488 nm (OG) and 647 (AF647) were used. Images were processed and analyzed with ImageJ (National Institutes of Health, Bethesda, MD). After a background correction (3), the classification of droplet and non-droplet pixels was done using the triangle automated thresholding algorithm in ImageJ (4). To quantitate phase separation, the fractional intensity $I_{frac}$ was calculated as the integrated intensity of pixels classified as part of droplets $I_{droplet}$ divided by the integrated intensity of all pixels $I_{all}$ within the image. Thresholding using the Huang method (5) in ImageJ gave very similar critical concentrations for phase separation.

**Fluorescence recovery after photobleaching (FRAP) on Rv1747$^{1\text{-}310}$ in solution**

FRAP studies of unmodified and phosphorylated OG-Rv1747$^{1\text{-}310}$ droplets, prepared in imaging chambers as described above, were carried out at ~ 22 °C (room temperature). The laser (473 nm) power was set to 5 % and the Tornado scanning tool (Olympus) was used. Fluorescence recovery was recorded at 1 frame/s for 180 to 500 s. The FRAP Profiler Plugin in ImageJ was used for intensity analysis and the normalization to the fluorescence intensity of a non-bleached area of the droplet. The recovery data of FRAP experiments on three different droplets within the same sample were averaged and analyzed in GraphPad Prism using a non-linear least squares fit to a single exponential recovery:

$$I(t) = I_{mobile}(1 - e^{-t/\tau})$$

Here, *I(t)* is the fractional intensity of the bleached region as a function of time, $I_{mobile}$ is the limiting intensity of the mobile fraction, and τ is the time constant for recovery. The latter was converted

to the half-time of recovery, $t_{1/2} = \tau/\ln 2$, the time it takes to recover half the mobile fraction intensity.

**Co-localization studies of Rv1747$^{1-310}$ droplets with PknF and PstP**

Non-labeled PknF catalytic domain at 0.5 μM was added to 50 μM samples of OG-Rv1747$^{1-310}$ in 20 mM sodium phosphate, 100 mM NaCl, 100 μM ATP, 5 mM $MgCl_2$ and 5 mM $MnCl_2$ at pH 7.4 to induce droplet formation. After 120 min, 0.05 μM AF647-labeled GST-PknF$^{1-292}$ or $His_6$-PstP$^{1-240}$ were added and images of OG (473 nm excitation) and AF647 (633 nm excitation) fluorescence taken and overlaid to monitor co-localization.

**Preparation and imaging of Rv1747$^{1-310}$ anchored on supported lipid bilayers**

Synthetic 1,2-dioleoyl-sn-glycero-3-phosphoethanolamine-N-[methoxy(polyethylene glycol)-5000] (ammonium salt, PEG5000-PE), 1,2-dioleoyl-sn-glycero-3- [(N-(5-amino-1-carboxypentyl)iminodiacetic acid)succinyl] (nickel salt, DGS-NTA($Ni^{2+}$)) and 1,2-dioleyl-sn-glycero-3-phosphocholine (POPC) were purchased from Avanti Polar Lipids. Mixtures of 0.1-10 % DGS-NTA-Ni, 99.8-89.9 % POPC and 0.1 % PEG5000-PE at 1 mg/mL total final lipid concentration were prepared in 1:1 v/v chloroform:methanol solvent. Glass coverslips (Marienfeld #1.5H, round, 18 mm; catalogue #0107032, Lauda-Königshofen, Germany) were rinsed with ethanol and double-distilled (dd) $H_2O$ and then treated with 1 % Hellmanex III solution in a sonication bath for 10 min. After another thorough rinse with dd$H_2O$, the cover slips were dried. The lipid mixture (40 μL) was added onto the clean cover slips, followed by spin-coating for 30 s at 2000 rpm using a Laurell WS-650 instrument. Any remaining solvent was evaporated for another 5 min. During that time, the cover slips were mounted in Chamlide CMB 18 mm Magnetic

Chambers (Live Cell Instruments) with 500 μL of buffer (20 mM sodium phosphate, 100 mM NaCl, pH 7.4) immediately after the drying period. Finally, 2 μM of $His_6$-tagged OG-$Rv1747^{1-310}$ was added to the imaging chambers and, after incubation for 10 min at 22 °C, the membrane clusters were investigated using confocal fluorescence microscopy as described above. FRAP studies of unmodified $Rv1747^{1-310}$ condensates anchored in supported lipid bilayers were carried out at ~ 22 °C (room temperature) using a 473 nm laser at 0.5 % power and the Tornado scanning tool (Olympus). Fluorescence recovery in this region was recorded at 1 frame/s for 150 s. The FRAP data were analyzed as above.

**Expression of msfGFP-tagged $Rv1747^{1-310}$ in yeast**

pRS313-GPDp-msfGFP-$Rv1747^{1-310}$-PGKt (BPM1451) was generated by Gibson assembly of the genes encoding and the yeast codon optimized *Mtb* $Rv1747^{1-310}$ into pRS313-GPDp-PGKt (BPM171). The resulting fusion protein included a tetrapeptide linker (SRPG) introduced between the N-terminal msfGFP and $Rv1747^{1-310}$. The monomeric superfolder fluorescent protein msfGFP is a derivative of sfGFP (6) with the V206K monomerizing mutation (a kind gift of Dr. S. Alberti). pRS313-GPDp-msfGFP-PGKt (BPM1452) was similarly generated as a control. Both plasmids were transformed into either the BY4741 strain (*MATa*, *his3Δ1*, *leu2Δ0*, *met15Δ0*, *ura3Δ0*) or a modified strain with a Nic96-mRFP nuclear envelope marker (YTM694: *MATa*, *his3Δ1*, *leu2Δ0*, *ura3Δ0*, *lys2Δ0*, *met15Δ0*, *nic96::NIC96-mRFP::KanMX6*). Cells were grown at 30 °C to mid-log phase ($OD_{600}$ ~ 0.6) in synthetic defined (SD) medium with LoFlo yeast nitrogen base (Formedium) and 2 % dextrose.

**Microscopy of yeast cells**

For epifluorescence microscopy, live BY4741 cells transformed with either of the above described plasmids were imaged for msfGFP localization using a Zeiss AxioObserver Z1 equipped with a 470 nm Colibri light source and a 63× 1.4 NA oil immersion DIC objective. Images were acquired and processed with the Zen2 software. For confocal microscopy, YTM694 (Nic96-mRFP) cells transformed with the either one of the two msfGFP plasmids were imaged with an inverted Zeiss Axiovert 200M microscope equipped with a QuantEM 512SC Photometrics camera and 100× 1.45 oil Plan-Fluor. Seven z-planes were acquired with 0.5 μm steps to detect msfGFP and mRFP localizations. Only a single z-plane was shown in each presented image.

**FRAP studies in yeast cells**

BY4741 cells expressing msfGFP-Rv1747$^{1\text{-}310}$ were imaged with an Olympus Fluoview FV1000 laser scanning confocal microscope with an UplanSApo 100× 1.40 oil immersion objective. The selected region of interest was photobleached with a 405 nm diode laser. Fluorescence recovery was recorded at 1 frame/5 s for 95 s. For FRAP analysis, the signal in the photobleached region was calculated after removing background signal (averaged from three region of interest in the field) and applying a photofading correction based on an exponential decay (averaged from three region of interest in adjacent non-bleached cells):

$$I(t) = I_0 e^{-t/\tau}$$

Here *I(t)* is the intensity at time *t*, $I_0$ is the initial intensity and τ is the decay time constant for fading. The data were averaged across three replicates after standardization and feature scaling in which the minimum and maximum signals were set to 0 and 1, respectively.

**Expression of mEos2-tagged Rv1747$^{1-310}$ and full-length Rv1747 in *M. smegmatis***

pJC52-mEos2 was generated by ligation of the acetamidase promoter and transcriptional start region from a pALACE shuttle vector (7) with the *mEos*2 gene, PCR-amplified from mEos2-C1 (Addgene #54510) into pMV261 lacking the HSP60 promoter. mEos2 is a bright photostable photoconvertable fluorescent protein (8). Codons encoding a $(SGGGG)_3$ linker, followed by a multiple cloning site, were also introduced downstream of the *mEos*2 gene. Finally, the genes encoding full-length Rv1747 or Rv1747$^{1-310}$ with a stop codon were ligated into the pJC52-mEos2 multiple cloning site to produce pJC52-mEos2-Rv1747 and pJC52-mEos2-Rv1747$^{1-310}$, respectively. These plasmids were confirmed by sequencing and transformed into *M. smegmatis* via electroporation.

**Microscopy of *M. smegmatis* cells**

For imaging, *M. smegmatis* harboring pJC52-mEos2, pJC52-mEos2-Rv1747$^{1-310}$, or pJC52-mEos2-Rv1747 were grown in Middlebrook 7H9 broth (BD Diagnostic Systems) with 0.2 % succincate, 0.05 % Tween-80, 20 μg/mL kanamycin and acetamide (0.2 %, 1 %, and 2 % for protein expression by the three strains, respectively) at 37 °C overnight to an $OD_{600}$ ~ 0.4 - 0.6. Live *M. smegmatis* cells were added to poly-L-lysine coated coverslips in a Chamlide magnetic chamber (Quorum Technologies; #CM-B18-1) that was assembled into a top-stage incubation system. All imaging was done at 37 °C with an Olympus TIRFM (Total internal reflection fluorescence microscope) system based on an inverted microscope (Olympus IX81) equipped with a 150x NA 1.45 TIRFM objective (Olympus), motorized filter wheel (Olympus), high performance electron multiplier (EM)-charge-coupled device (CCD) camera (Photometrics Evolve), and real-time data acquisition software (Metamorph). The 491 nm solid-state diode lasers were used to excite mEos2. The TIRF plane was adjusted to yield a penetration depth of ~ 150 nm from the

coverslip and TIRF imaging was carried out for 10 s at 33 frames/s. Individual particles/foci were then detected using Icy Bioimaging analysis software (9). Particle detection for binary (0 or 1) images was done using the UnDecimated Wavelet Transform Detector plugin, which was set to detect bright spots over a dark background, exhibit 50 % sensitivity to spots < 3 pixels, and apply size filtration in order to detect objects ranging from 2 pixels to 3000 pixels.

**FRAP of mEos2-Rv1747$^{1-310}$ in *M. smegmatis***

Images were acquired using an Olympus Fluoview FV1000 laser scanning confocal microscope with an UplanSApo 100× 1.40 oil immersion objective. The selected region of interest was photobleached with a 405 nm diode laser, and images were acquired every 3 seconds for 20 frames. The background intensity measurement confirmed complete photobleaching of fluorescent signal at the region of interest. A region in the midpoint of the bacteria was used to quantify FLIP (fluorescence loss in photobleaching). An additional region of interest from adjacent non-bleached bacterium was used to correct for photofading. For FRAP analysis, the signal intensities in the selected regions were quantified using ImageJ. The values were then normalized to the first frame of the corresponding image stack.

**Selection of single chain variable fragment (scFv) specific for Rv1747$^{1-156}$**

Selection, production and purification of the scFv was carried out by the Antibody Engineering Facility at the UBC Immunity and Infection Research Centre (IIRC) as described previously (10). Briefly, Rv1747$^{1-156}$ (FHA-1 and partial linker) was used for biopanning against an optimized M13 bacteriophage phagemid library presenting ~ $10^9$ different scFv clones fused to the major viral coat protein g3p. The scFv's with affinity to Rv1747$^{1-156}$ were eluted after washing

and enriched by repeating the biopanning process three times. The highest affinity scFv, as judged by an enzyme linked immunosorbent assay (ELISA), was used for studies presented herein. After production in *E. coli* and purification, the scFv was labelled non-specifically at exposed amines with an N-hydroxysuccinimide-functionalized AF647 fluorescent dye by the AbLab at the UBC Biomedical Research Centre.

**Co-localization studies of scFv's with Rv1747$^{1-310}$ droplets**

Non-labeled PknF at 0.5 μM was added to 50 μM samples of OG-Rv1747$^{1-310}$ in 20 mM sodium phosphate, 100 mM NaCl, 100 μM ATP, 5 mM $MgCl_2$ and 5 mM $MnCl_2$ at pH 7.4 to induce droplet formation. After 120 min, 0.05 μM of Rv1747-specific or a non-specific scFv were added, both being AF647-labeled. The latter control was selected against a eukaryotic protein without any *Mtb* homolog. Images of OG and AF647 fluorescence taken and overlaid to monitor co-localization.

**Growth, preparation and labeling of *Mtb* for Single-molecule Localization Microscopy (SMLM)**

All protocols for *Mtb* manipulation were approved by the University of British Columbia and carried out in accordance with institutional regulations. *M. tuberculosis* H37Rv (harboring GFP-expressing pTEC15) and Erdman strains were grown in 7H9 broth supplemented with 10 % (v/v) OADC (oleic acid, albumin, dextrose and catalase solution) and 0.05 % (v/v) Tween-80 (Sigma-Aldrich) at 37 °C in standing cultures. The Δ*rv1747* Erdman mutant (11) was additionally grown with 50 μg/mL hygromycin. Bacteria were cell wall-labeled by adding 100 μM tag (12) to cultures grown to $OD_{600}$ ~ 0.5 and incubated overnight at 37 °C. Cells were washed three times

with phosphate buffer saline (PBS) and 0.05 % Tween-80, washed once with PBS, and resuspended in PBS. Acid-cleaned glass coverslips (Marienfeld #1.5H,18 × 18 mm; #0107032, Lauda-Königshofen, Germany) were incubated with 0.01% poly-L-lysine (Sigma-Aldrich; #P4707) for at least 1 h at 37°C, followed by PBS washing. *Mtb* (50 µL containing ~ $5\times10^7$ cells) were added onto the poly-L-lysine coated coverslips, allowed to adhere for 2 hours at room temperature, and subsequently fixed with PBS containing 4% paraformaldehyde (PFA) for 30 minutes.

Coverslips were washed thoroughly with PBS and processed for intracellular staining, as previously described (13). Briefly, *Mtb* samples were first treated with lysozyme (Sigma Aldrich 10837059001**,** 2 mg/ml in $H_2O$) for 30 min at 37 °C, followed by Triton X-100 (0.1 % in $H_2O$) for 5 min at ~ 22 °C. After PBS washes, the sample was blocked with 10 % normal goat serum in PBS for 30 min and stained with the AF647-conjugated Rv1747-specific or non-specific scFv for 1 h at 22 °C. The coverslips were washed with PBS before adding fiducial markers (F8799, ThermoFisher Scientific) for image stabilization and incubating overnight at 4 °C.

**Confocal imaging of *Mtb* and the Δ*rv1747* Erdman mutant**

Imaging of *Mtb* and the Δ*rv1747* Erdman mutant was performed using a spinning disk confocal microscope system (Intelligent Imaging Innovations) consisting of a Zeiss Axiovert 200M microscope with a 100 X NA 1.45 oil Pan-Fluor objective and a QuantEM 512SC Photometrics camera.

**SMLM image acquisition and reconstruction**

SMLM imaging was carried out using a custom-built microscope with a real-time sample drift-stabilization system that has been described previously (14, 15). Briefly, three lasers were used in the excitation path: a 639 nm laser (Genesis MX639, Coherent) for exciting AF647, a 488 nm laser (DHOM-100B, Fine Mechanics) for exciting GFP, and a 405 nm laser (LRD 0405, Laserglow Technologies) for reactivating AF647. All three lasers were coupled into an inverted microscope equipped with an apochromatic TIRF oil-immersion objective lens (60× 1.49 NA; Nikon). The fluorescence was separated using dichroic mirrors and filters (Semrock), and detected by EM-CCD cameras (iXon, Andor). A feedback loop was engaged to lock the position of the sample during image acquisition (14, 15). Sample drift was controlled to be less than 1 nm laterally and 3 nm axially.

Imaging was performed in oxygen-scavenging GLOX-thiol buffer (50 mM Tris-HCl, 10 mM NaCl, 0.5 mg/ml glucose oxidase, 40 µg/ml catalase, 10% (w/v) glucose, 140 mM 2-mercaptoethanol, pH 8.0) (16). The coverslip with attached scFv-stained *Mtb* was mounted onto a depression slide filled with imaging buffer and sealed with Twinsil two-component silicone-glue (#13001000, Picodent). For SMLM imaging, cells were exposed to a laser power density of 1 kW/cm$^2$ for the 639 nm laser to activate the AF647. For each reconstructed SMLM image, 40000 images were acquired at 50 Hz. Custom software written in MATLAB (Mathworks) was used to reconstruct the SMLM images (14).

**DBSCAN cluster analysis and calculation for higher order multimers**

Clustering of SMLM localizations was performed in 3D using DBSCAN (17). Prior to clustering, the axial (z) dimension of the data was rescaled so that uncertainties in the z-coordinates

of localizations were comparable to those in the x- and y-coordinates. Although DBSCAN does not account for localization uncertainties, rescaling the z-dimension ensured that the increased uncertainty in the z-coordinates did not unduly contribute to clustering results. The areas of clusters (projected onto the xy-plane) were determined using the MATLAB function "boundary" with the default "shrink factor" of 0.5. Various DBSCAN parameters, based on the minimum number (MinPts) of localizations within a distance cut-off (Eps) of each other, were used for defining clusters with DBSCAN and yielded consistent results (*SI Appendix*, Fig. S15*B*).

To estimate the area above which clustering was taken as multimerization, we used the sum of the sizes for all components of the regulatory module of Rv1747 (*SI Appendix*, Fig. S15*A*). This included the end-to-end distance of a flexible linker between the FHA domains (~ 8.3 nm), the diameters of FHA domains (2 × ~ 3.3 nm) and scFv (~ 3.8 nm), and a localization error of ~ 10 nm. The root-mean-squared end-to-end distance $\langle r^2 \rangle^{1/2}$ of the intervening linker was calculated using a predicted radius of gyration $R_g$ of 3.4 nm according to (18) and assuming a Gaussian chain, resulting in the relationship $R_g^2 = 1/6 \times \langle r^2 \rangle$ (19). The length of the entire regulatory module was thereby estimated as ~ 28.7 nm and considered to be the maximum distance of a fluorescent signal from the center of the Rv1747 transporter pore. This was used to calculate the maximum circular area of ~ 2600 $nm^2$ covered by this flexible "arm".

**Supplemental Figures**

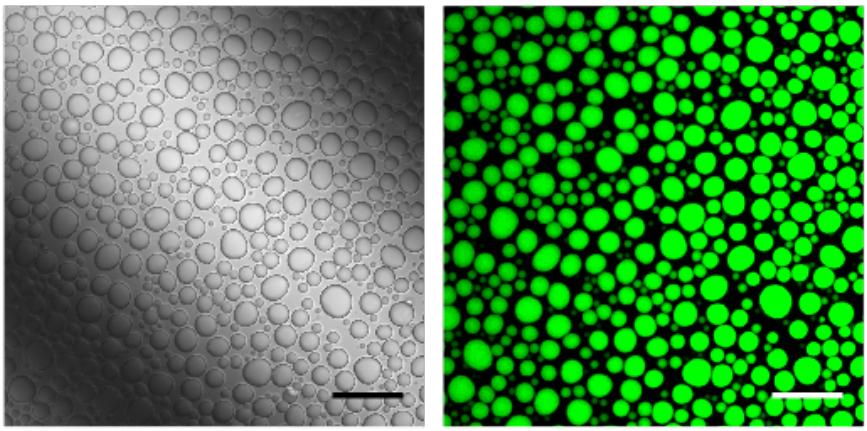

**Fig. S1. Rv1747$^{1-310}$ undergoes phase separation *in vitro* upon phosphorylation.** Rv1747$^{1-310}$ (50 μM) forms droplets upon phosphorylation by 5 μM PknF in buffer containing 5 mM ATP. Shown are differential interference contrast (DIC; left) and fluorescence microscopy (right) images, acquired consecutively on the same sample of Oregon Green (OG) labeled protein at room temperature (~ 22 °C) (scale bars: 20 μm). The observation of uniformly fluorescent droplets confirmed that Rv1747$^{1-310}$ was the main constituent of these condensates.

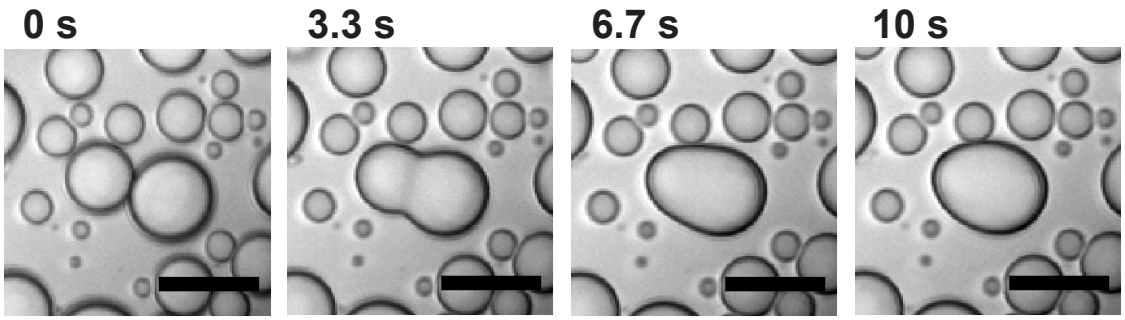


**Fig. S2. Coalescence of Rv1747$^{1-310}$ droplets.** DIC images showing the time course for coalescence of two Rv1747$^{1-310}$ droplets (~ 22 °C). The droplets were formed by addition of 0.5 μM PknF to 50 μM Rv1747$^{1-310}$ in buffer containing 100 μM ATP. Time t = 0 s corresponds to the start of image collection (scale bars: 5 μm).

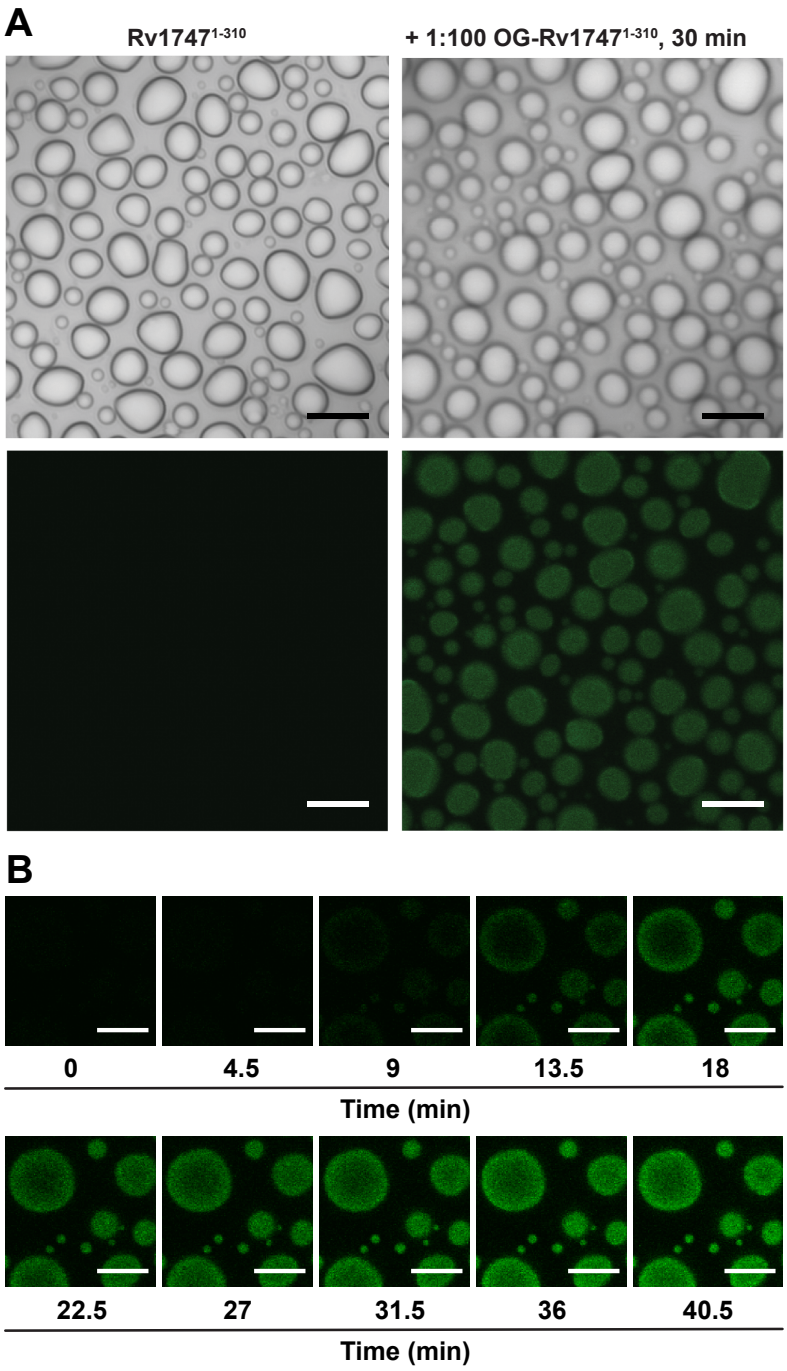


**Fig. S3. Diffusive exchange occurs from the protein-depleted to the protein-rich phases of an Rv1747$^{1-310}$ sample.** (*A*, left) Shown are DIC (top) and fluorescent images (bottom) of non-fluorescent, phosphorylated Rv1747$^{1-310}$ droplets formed at 50 μM by addition of 0.5 μM PknF

and 100 μM ATP. (*A*, right) Similar images were recorded 30 min after the addition of 0.5 μM non-phosphorylated OG-Rv1747$^{1-310}$. Incorporation of the fluorescent OG-labeled protein into the previously non-fluorescent droplets can be seen (scale bars: 5 μm). (*B*) Representative fluorescence images taken at different time points after addition of OG-Rv1747$^{1-310}$ to the preformed droplets at 22 °C as in (*A*) (scale bars: 5 μm). The relatively slow rate of incorporation compared to FRAP recovery times is attributed to the low concentration of OG-Rv1747$^{1-310}$ in solution. Under these conditions, even if phosphorylated by PknF, the OG-Rv1747$^{1-310}$ is too dilute to form new droplets. It was not determined if the OG-Rv1747$^{1-310}$ incorporated into the existing droplets was unmodified or phosphorylated by PknF using ATP remaining in solution.

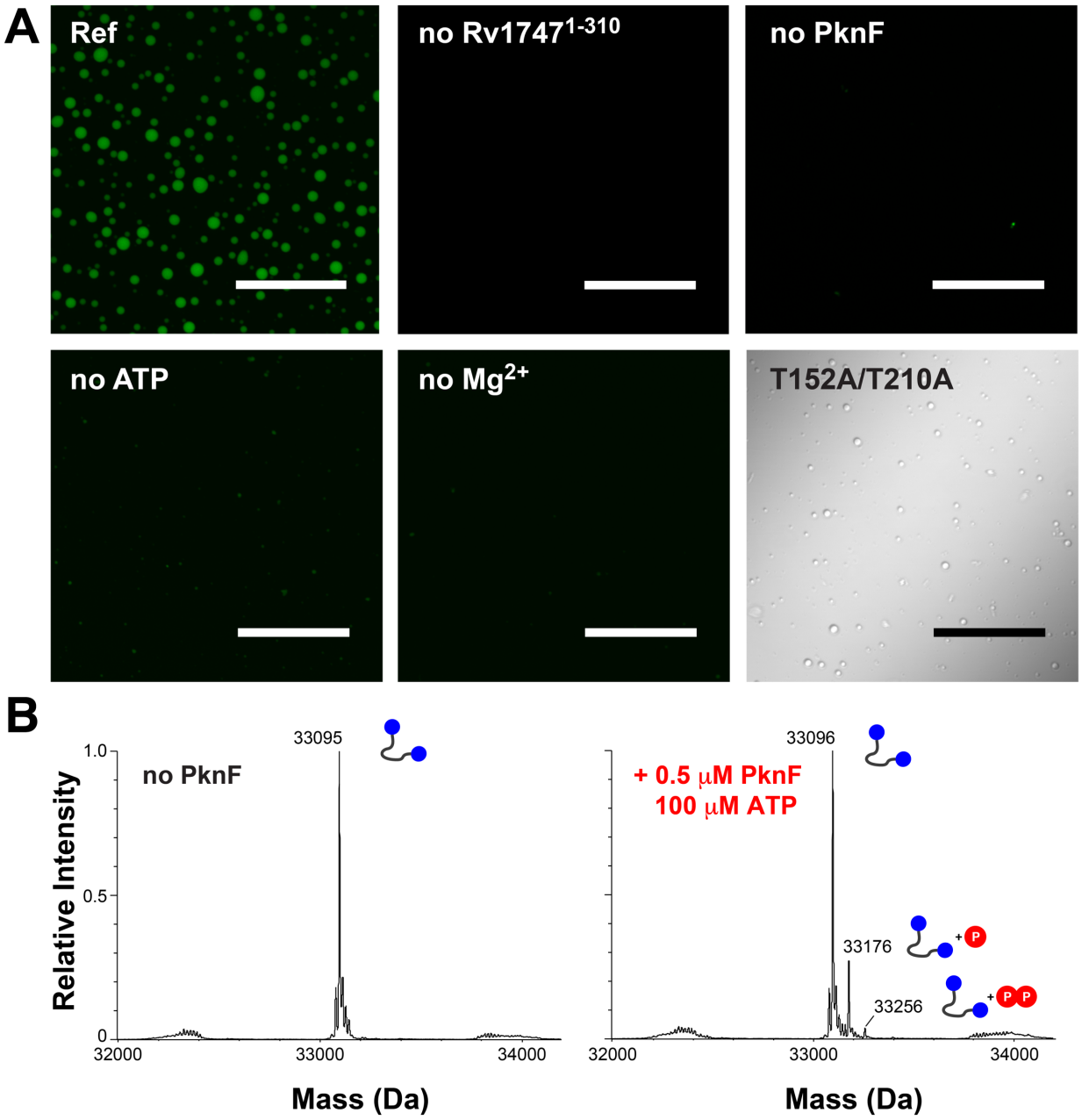


**Fig. S4. Sub-stoichiometric phosphorylation of Rv1747$^{1-310}$ by PknF is sufficient to induce phase separation.** (*A*) Reference fluorescence image of 50 μM OG-labeled Rv1747$^{1-310}$ droplets, formed in buffer containing 0.5 μM PknF, 100 μM ATP and 5 mM $Mg^{2+}$. Also shown are fluorescence images of controls where the indicated component was omitted. The DIC image

(lower right) corresponds to unlabeled Rv1747$^{1-310}$ with the phospho-ablative T152A/T210A mutations subjected to the same conditions (scale bars: 20 μm). Despite mutation of the two mapped phospho-acceptor threonine residues, some droplet formation still occurred, albeit much less efficiently, presumably due to phosphorylation of alternative linker sites (*SI Appendix*, Fig. S6; see also *SI Appendix*, Figs. S5 and S10). Note that 50 μM is below the threshold concentration of ~ 250 μM for phase separation by unmodified Rv1747$^{1-310}$. (*B*) ESI-MS of Rv1747$^{1-310}$ before phosphorylation (left) and after 120 min of treatment with PknF (right) under the conditions used in (*A*). Masses of major peaks are indicated and the corresponding phosphorylation states are shown as cartoons with phosphates and FHA domains represented in red and blue, respectively. Under these conditions, the PknF-treated protein was predominantly unmodified, with ~ 20 % single-phosphorylated and a small amount of double-phosphorylated forms also present. These ESI-MS measurements were carried out with thoroughly re-suspended samples, and thus possible differences in the phosphorylation states of Rv1747$^{1-310}$ within the droplets versus in solution were not determined.

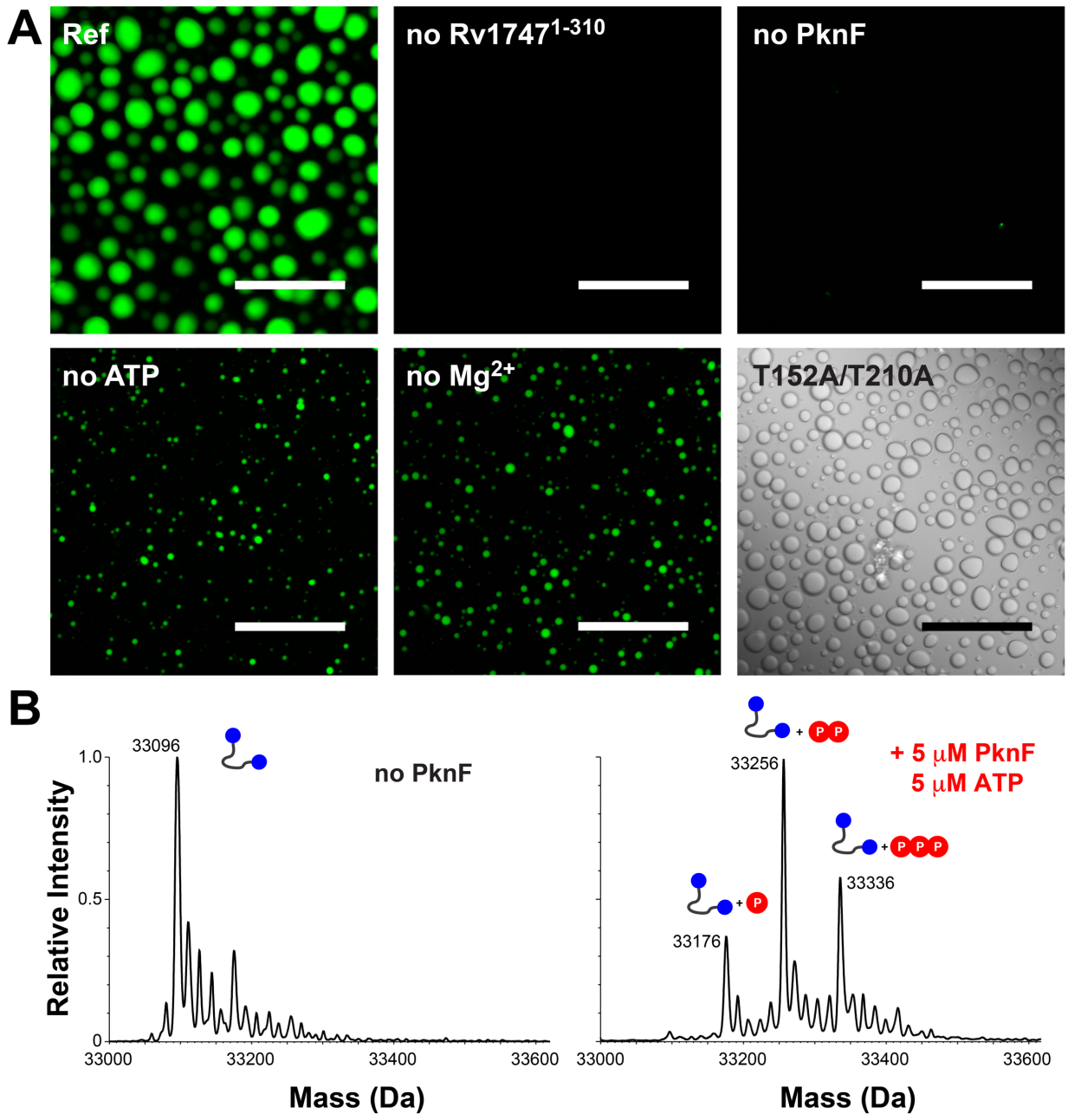


**Fig. S5. High concentrations of PknF with excess ATP phosphorylate Rv1747$^{1-310}$ at additional sites that also contribute to phase separation.** (*A*) Reference fluorescence image of OG-Rv1747$^{1-310}$ droplets, formed at 50 μM in buffer containing 5 mM $Mg^{2+}$ and 5 mM ATP treated with 5 μM PknF. Also shown are fluorescence images of controls where the indicated component

was omitted. The small droplets formed in the absence of added ATP or $Mg^{+2}$ are attributed to sub-stoichiometric phosphorylation of $Rv1747^{1-310}$ by the high concentration of added active kinase, heterologously-expressed in the presence of $Mg^{2+}$ and ATP in *E. coli*. The DIC image is of unlabeled $Rv1747^{1-310}$ T152A/T210A subjected to the same conditions (scale bars: 20 μm). Although lacking T152 and T210, droplets still formed due to phosphorylation at additional mapped sites (*SI Appendix*, Fig. S6; see also *SI Appendix*, Figs. S4 and S10). Note that 50 μM is below the threshold concentration of ~ 250 μM for phase separation by unmodified $Rv1747^{1-310}$. (*B*) ESI-MS of $Rv1747^{1-310}$ before phosphorylation and after 120 min of treatment with PknF under the conditions used in (*A*). Masses of major peaks are indicated and the corresponding phosphorylation states are shown as a cartoons with phosphates represented by red circles. The PknF-treated protein is a mixture of at least single-, double- and triple-phosphorylated forms. Thus phosphorylation can occur at sites other than the previously reported phospho-acceptors T152 and T210 (20). As with *SI Appendix*, Fig. S4, the ESI-MS measurements were carried out with thoroughly re-suspended samples, and possible differences in the phosphorylation states of $Rv1747^{1-310}$ within the droplets versus in solution were not determined.

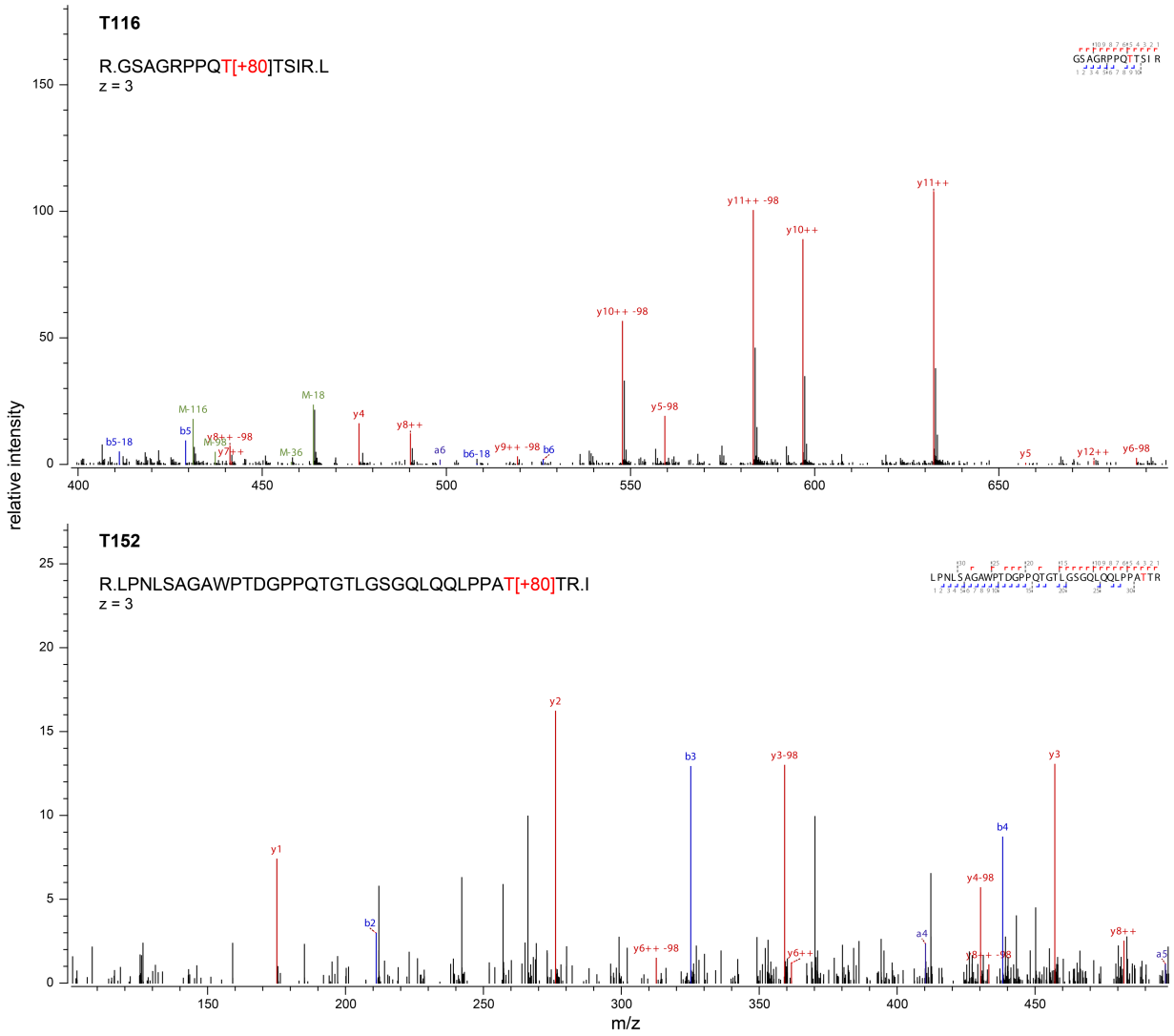


**Fig. S6. Identification of phospho-acceptor sites in Rv1747$^{1-310}$ phosphorylated by PknF.** MS/MS spectra of phosphorylated peptides GSAGRPPQTTSIR (top) and LPNLSAGAWPTDGPPQTGTLGSGQLQQLPPATTR (bottom). The spectra are displayed over the m/z ranges that show the key fragment ions necessary to localize the sites of phosphorylation to the highlighted residues T116 and T152, respectively. Similar data were obtained for the additional PknF phospho-acceptors T117, S161 and T169.

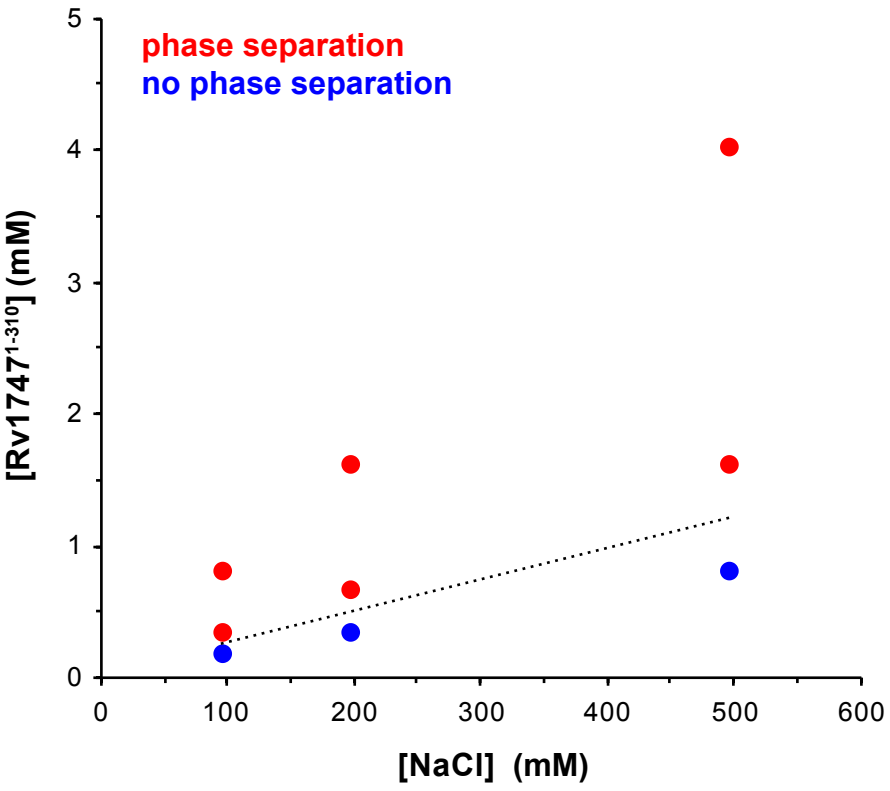


**Fig. S7. The saturation concentration for phase separation of non-phosphorylated Rv1747$^{1-310}$ increases with ionic strength.** Phase diagram of OG-Rv1747$^{1-310}$ as a function of NaCl concentration. Red/blue indicate the presence/absence of droplets with a fractional fluorescent intensity > 0.5. Protein solutions were dialyzed against buffer (20 mM sodium phosphate, pH 6) with varying [NaCl] for 24 h and imaged by fluorescence microscopy at room temperature after thorough resuspension. Note that at each [NaCl], three samples of OG-Rv1747$^{1-310}$ at the indicated final concentrations were examined. The dashed line shows the approximate protein saturation concentration for phase separation as a function of [NaCl]. These results demonstrate that electrostatic interactions contribute to the phase separation of unmodified Rv1747$^{1-310}$.

**Rv1747$^{1-310}$**

```
        10         20         30         40         50
MPMSQPAAPP VLTVRYEGSE RTFAAGHDVV VGRDLRADVR VAHPLISRAH
        60         70         80         90        100
LLLRFDQGRW VAIDNGSLNG LYLNNRRVPV VDIYDAQRVH IGNPDGPALD
       110        120        130        140        150
FEVGRHRGSA GRPPQTTSIR LPNLSAGAWP TDGPPQTGTL GSGQLQQLPP
                  **
       160        170        180        190        200
ATTRIPAAPP SGPQPRYPTG GQQLWPPSGP QRAPQIYRPP TAAPPPAGAR
 *         *        *
       210        220        230        240        250
GGTEAGNLAT SMMKILRPGR LTGELPPGAV RIGRANDNDI VIPEVLASRH
       260        270        280        290        300
HATLVPTPGG TEIRDNRSIN GTFVNGARVD AALLHDGDVV TIGNIDLVFA
       310
DGTLARREEN
```

**MSMEG_1642$^{1-340}$**

```
        10         20         30         40         50
MSRPSPPALT VRYEGSTRTF APGSDVVIGR DLRADVRIAH PLISRAHLVL
        60         70         80         90        100
RFDQGRWVAI DNGSLNGMYV NGRRVSSVDL QDGQVLNIGN PDGPQLSFEV
       110        120        130        140        150
GRHQGSAGRT PTAAVPVAGH TGTSWPTQAP TGGGWQQPYT QPPRTQYPQT
       160        170        180        190        200
TGTQQRYPSA PQHGYPNGPQ TGYPSGPQRG YPSGPQTGYP TNGPAGAPQS
       210        220        230        240        250
YQSQPVRTPP PAPANSSQAP TTMGPAAAPR GGAEPASNLA TSMLKILRPG
       260        270        280        290        300
RSAPAPAGAV KIGRATDNDI VIPDVLASRH HATLIPLPGG TEIRDERSIN
       310        320        330        340
GTFVNGTRVD SAVLHDGDVV TIGNVDLVFS GGTLARRSET
```

**Fig. S8. Sequence analysis of Rv1747$^{1-310}$ and MSMEG_1642$^{1=340}$.** The sequences of the Rv1747 and MSEMG_1642 regulatory modules are shown. Residues forming the two structured FHA domains are in brown font (defined structurally for Rv1747 (21) and predicted for MSMEG_1642). Within the intrinsically disordered linker, positively (red) and negatively (blue) charged residues are indicated, along with aromatic residues (green), glycines (cyan), and threonines (magenta). The two previously reported phospho-acceptor threonines, Thr152 and Thr210, for PknF in Rv1747 are highlighted in yellow (20), and those identified herein are indicated with an *.

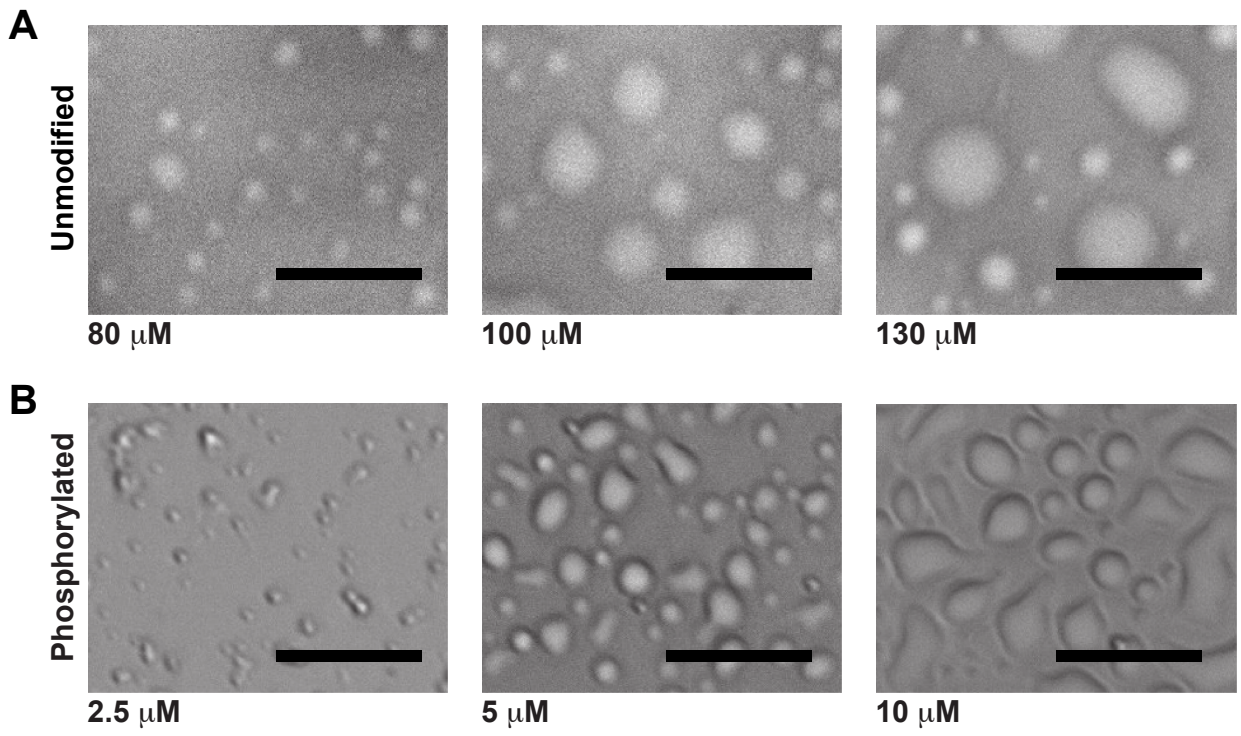


**Fig. S9. MSMEG_1642$^{1-340}$ also undergoes phosphorylation-enhanced phase separation.** (*A*) DIC images of unmodified $His_6$-tagged MSMEG_1642$^{1-340}$ recorded approximately 120 min after concentration to the indicated values (100 mM NaCl, 20 mM sodium phosphate, pH 6 at room temperature). Under these conditions, droplets formed at a saturation concentration of ~ 100 μM. (*B*) Phosphorylation by PknF (120 min treatment with 0.5 μM kinase, 100 μM ATP, 5 mM $MgCl_2$, 100 mM NaCl, 20 mM sodium phosphate, pH 6) reduced the threshold concentration to ~ 5 μM (scale bars: 20 μm).

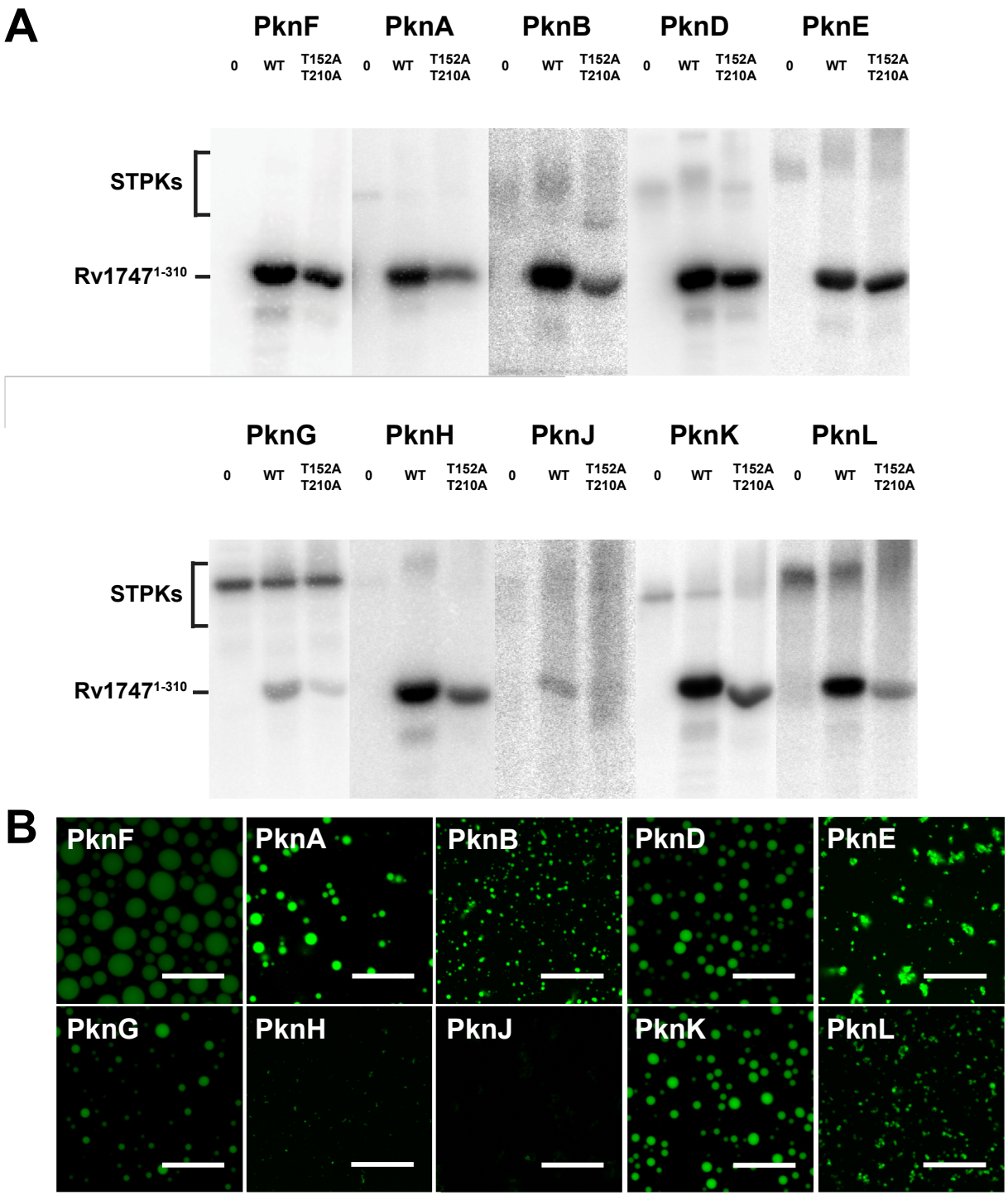


**Fig. S10. Several *Mtb* STPKs phosphorylate Rv1747$^{1-310}$ at multiple sites and induce phase separation.** (*A*) Autoradiograms of SDS-PAGE gels of 10 μM Rv1747$^{1-310}$ or Rv1747$^{1-310}$ T152A/T210A phosphorylated by 0.5 - 2 μM of the kinase domains of ten *Mtb* STPKs (5 μCi of

[γ-$^{32}$P]ATP, 5 mM $Mg^{2+}$ and 5 mM $Mn^{2+}$). The T152A/T210A variant is still phosphorylated to varying degrees at additional unmapped sites. Control lanes (0) without Rv1747$^{1-310}$ are included. Predicted sizes of Rv1747$^{1-310}$ and the autophosphorylated STPKs are indicated. (*B*) Fluorescence images of OG-Rv1747$^{1-310}$ droplets formed by these STPKs under the same conditions as in (*A*) except using 100 μM of non-radioactive ATP. At this concentration of 10 μM, unmodified Rv1747$^{1-310}$ does not phase separate (scale bars: 20 μm). A close inspection of the fluorescence images reveals droplets with a range of different droplet morphologies. For example, phosphorylation of Rv1747$^{1-310}$ by PknB and PknD resulted in phase separation to small spherical droplets, whereas those induced by PknE and PknL had non-spherical shapes. Such differences in the material properties of phase-separated Rv1747$^{1-310}$ may arise from differences in the stoichiometry and sites of phosphorylation associated with each particular STPK.

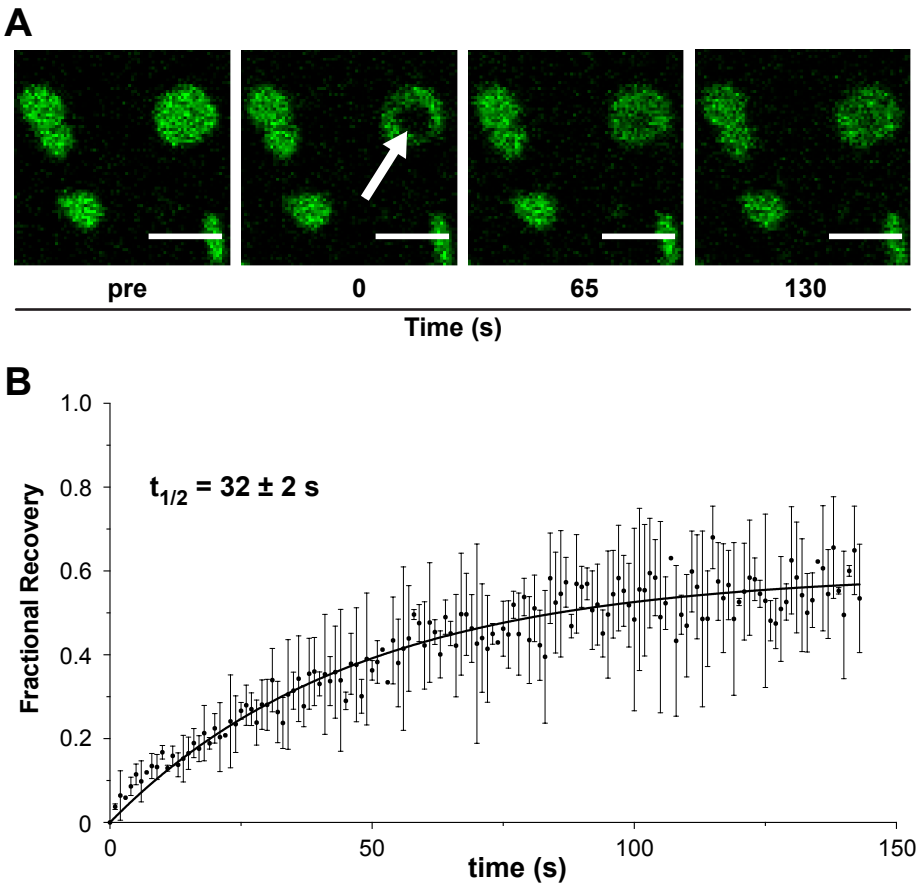


**Fig. S11. Diffusive exchange of Rv1747$^{1-310}$ clusters on supported lipid bilayers characterized by FRAP.** Condensates of non-phosphorylated His$_6$-tagged OG-Rv1747$^{1-310}$ anchored on supported lipid bilayers (SLBs) also exhibit diffusive exchange. The SLBs were formed as in Fig. 4 with 2 % DGS-NTA(Ni$^{2+}$) in the lipid mixture. (*A*) The bleached sector is indicated by an arrow in the t = 0 image, followed by representative images taken at two subsequent time points (~ 22 °C, scale bars: 3 μm). (*B*) Recovery was quantified by fitting the average normalized intensity (solid dots with grey bars showing standard deviations) of FRAP measurements on two different membrane-anchored, unmodified condensates of Rv1747$^{1-310}$ from the same sample to a single exponential function (black line). The $t_{1/2}$ to 50 % recovery of the mobile fraction was 32 ± 2 s.

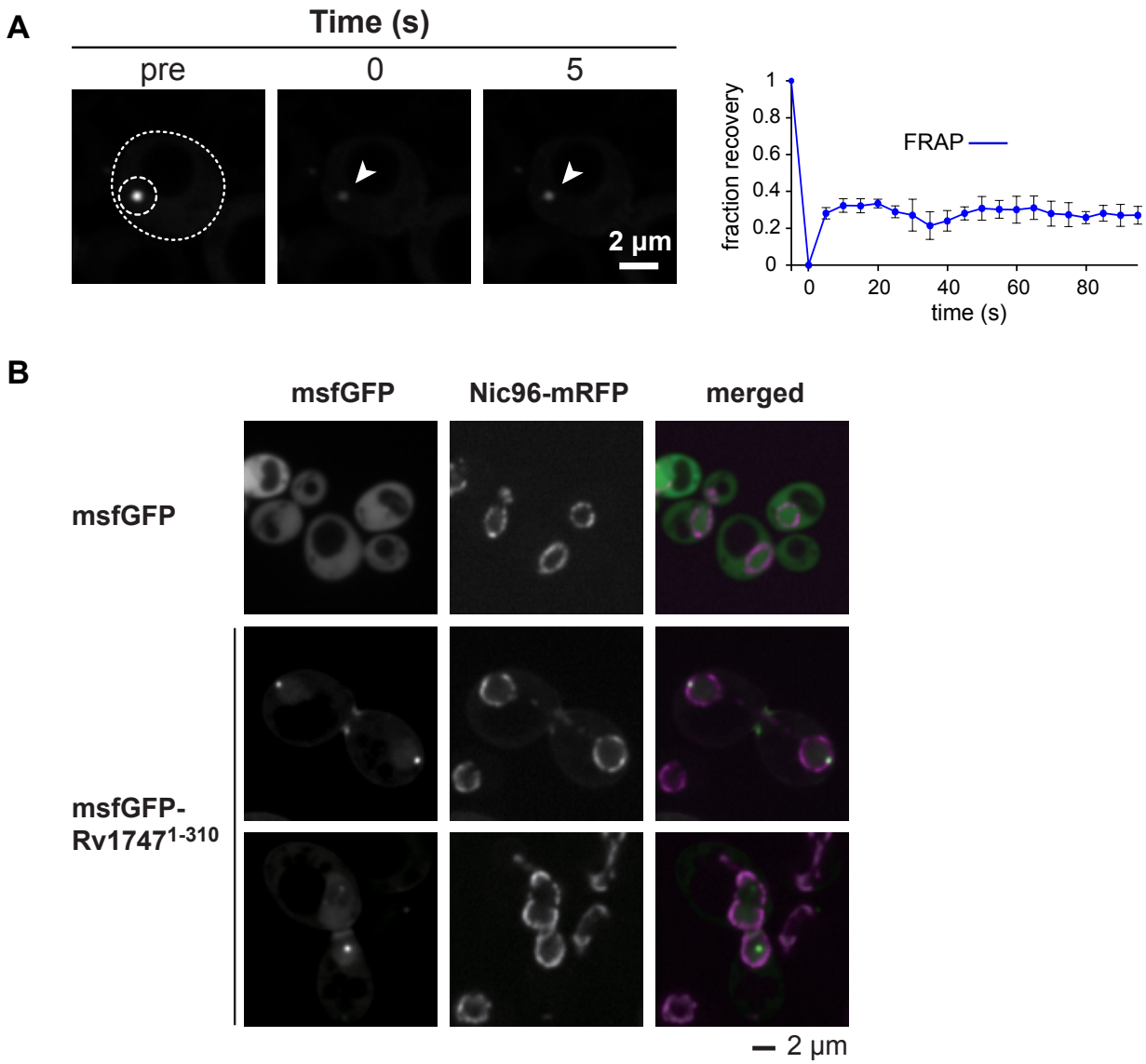


**Fig. S12. Foci formation by Rv1747$^{1-310}$ in *S. cerevisiae.*** (*A*) FRAP of msfGFP-Rv1747$^{1-310}$ foci. The region of interest in a representative cell (large dashed circle) is delimitated by the small dashed circle in the pre-bleached image, and the arrowhead identifies the foci in the t = 0 and t = 5 sec images. The plot shows the averaged FRAP results on three different foci of Rv1747$^{1-310}$. Although initial recovery is quick, only ~ 30 % of the total fluorescence is regained. Detailed inspection revealed that yeast cells generally have only one msfGFP-Rv1747$^{1-310}$ focus that is

localized in the nucleus (see next panel), which therefore limits the amount of protein available for recovery after photobleaching. (B) Representative confocal images of msfGFP alone (top row) and msfGFP-Rv17471-310 (middle and lower rows) in Nic96-mRFP expressing cells. Imaging of msfGFP-Rv17471-310 showed a slight increase of the msfGFP signal near the foci that was consistent with a possible nuclear localization (see Fig. 4*B*). To test this possibility, we repeated the imaging with Nic96-mRFP, a component of the nuclear pore complex. The left (msfGFP fluorescence) and middle (mRFP fluorescence) columns are presented in black and white for contrast. The merged images (right column) show that the msfGFP (green) alone is uniformly distributed in the cytoplasm, whereas msfGFP-Rv1747$^{1-310}$ (green) forms foci located in the nucleus as marked with Nic96-mRFP (magenta).

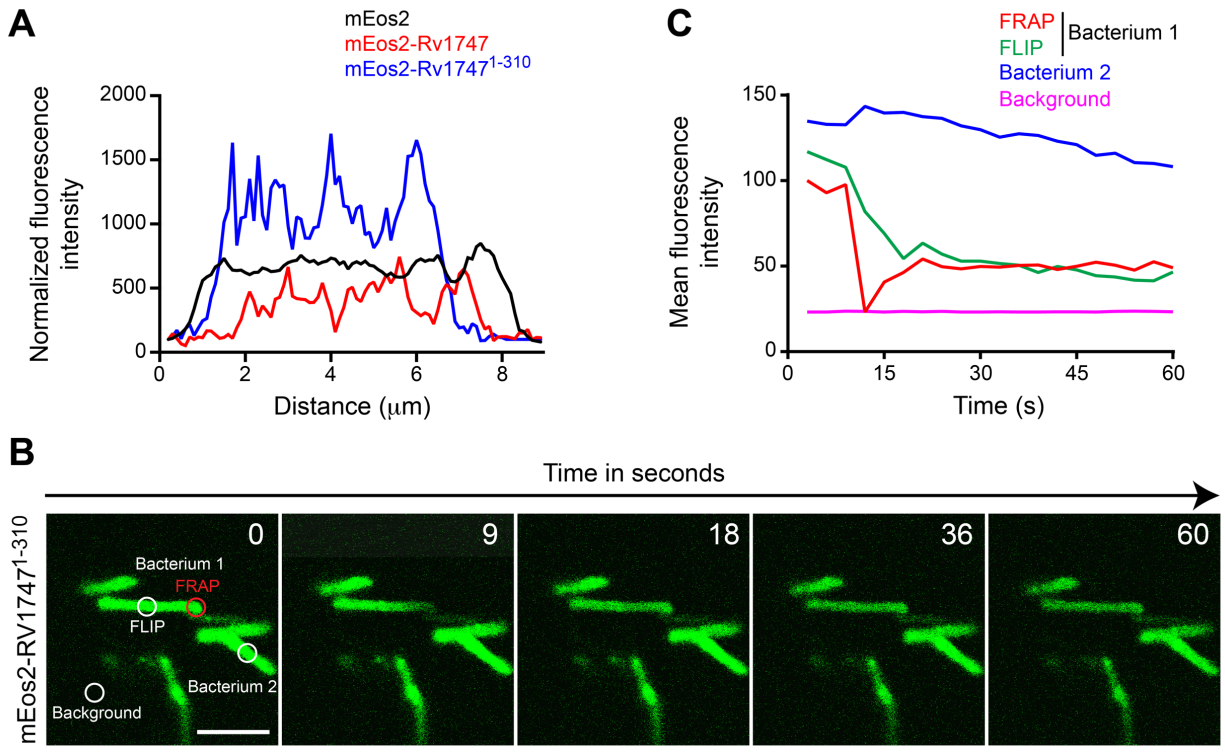


**Fig. S13. Dynamic foci formation by Rv1747$^{1-310}$ and Rv1747 in *M. smegmatis*.** (*A*) Intensity profiles of fluorescence as measured along the length of each bacterium, shown in the upper left panels of Fig. 4*C*. The mEos2 signal intensity is uniform and remains largely unchanged throughout the length of the bacterium. In contrast, the mEos2-Rv1747$^{1-310}$ and mEos2-Rv1747 signal intensities vary, indicating the clustering of proteins. The values are normalized to the corresponding background signal intensity outside the bacteria, and set to an arbitrary value of 100. (*B*) Representative image stacks from a FRAP experiment on *M. smegmatis* expressing mEos2-Rv1747$^{1-310}$. The FRAP and FLIP (Fluorescence Loss in Photobleaching) regions of bacterium 1, non-photobleached region of bacterium 2 and background region used for image quantification are indicated (scale bar = 5 μm). (*C*) Fluorescence intensity values as measured from the indicated regions in B. All values are normalized to the first frame of the photo-bleached region, which is set to an arbitrary value of 100.

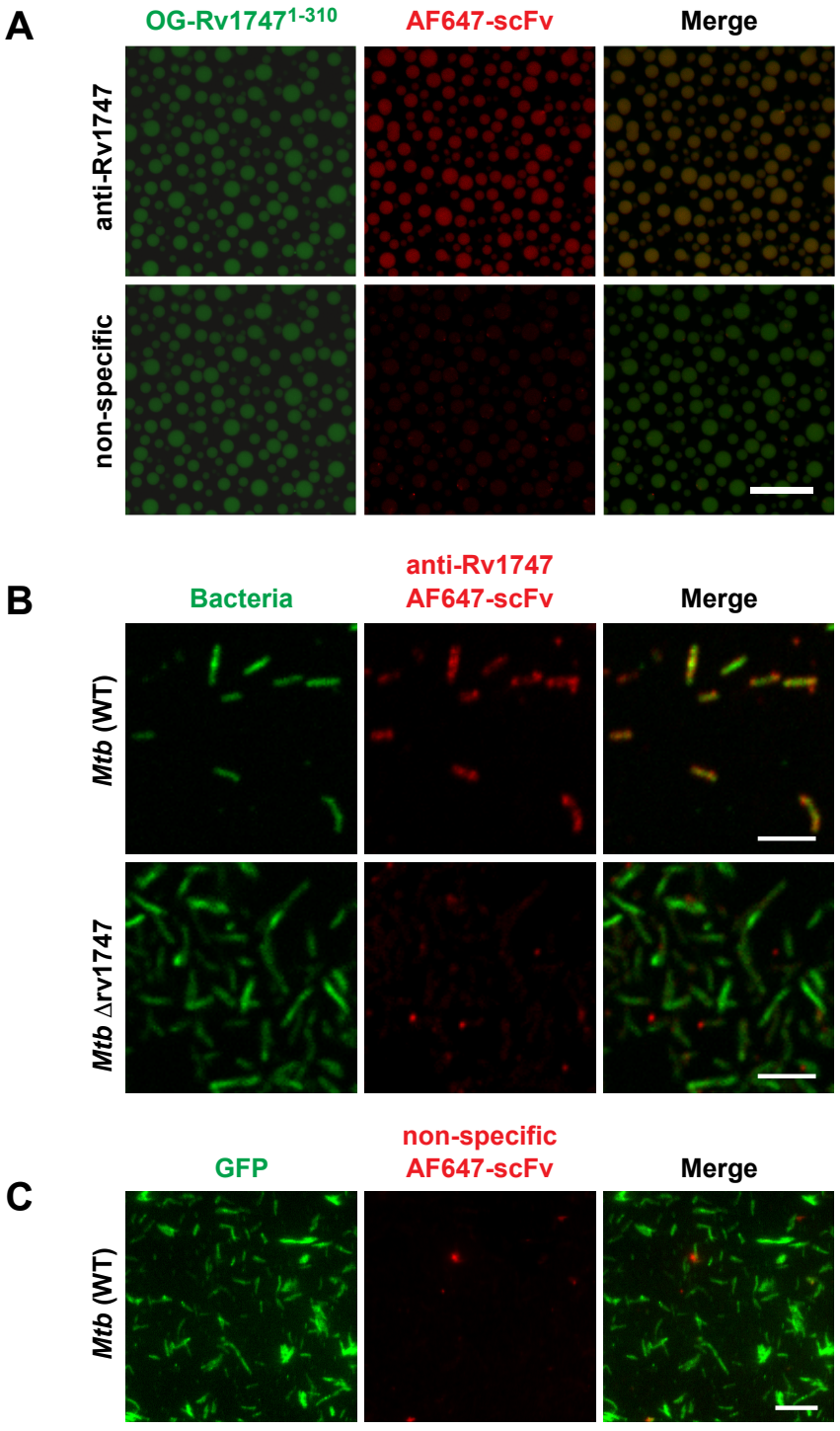


**Fig. S14. Controls for single chain variable fragment (scFv) selected against the FHA-1.** (A) Top, condensates of OG-Rv1747$^{1-310}$ (50 μM) were formed in buffer containing 0.5 μM PknF with

100 μM ATP. Subsequently, 0.05 μM of an AF647-labeled scFv, selected in a phage display screen to bind the Rv1747 FHA-1 domain, was added. OG (green) and AF647 (red) fluorescence was measured and overlaid to show co-localization. Bottom, as a control, the same experiment was repeated with a "non-specific" AF647-scFv that differs from the R1747-specific AF647-scFv only in the complementarity-determining regions. In this case, no staining was observed (scale bars: 20 μm). *(B)* Representative confocal micrographs of cell-wall labeled (green) *Mtb* and Δ*rv1747* treated with the Rv1747-specific AF647-scFv (red; scale bar = 5 μm). The specific scFv stained only fixed, permeabilized *Mtb* cells expressing Rv1747 and not the Δ*rv1747* cells. The middle column of this panel is shown in Fig. 5*A*. *(C)* Unlike the scFv specifically selected against the FHA-1 domain of Rv1747, the non-specific scFv did not stain *Mtb*. Representative Total Internal Reflection Fluorescence (TIRF) micrographs of fixed, permeabilized GFP-expressing *Mtb* cells (green) treated with a non-specific AF647-labeled scFv (red, scale bar: 10 μm).

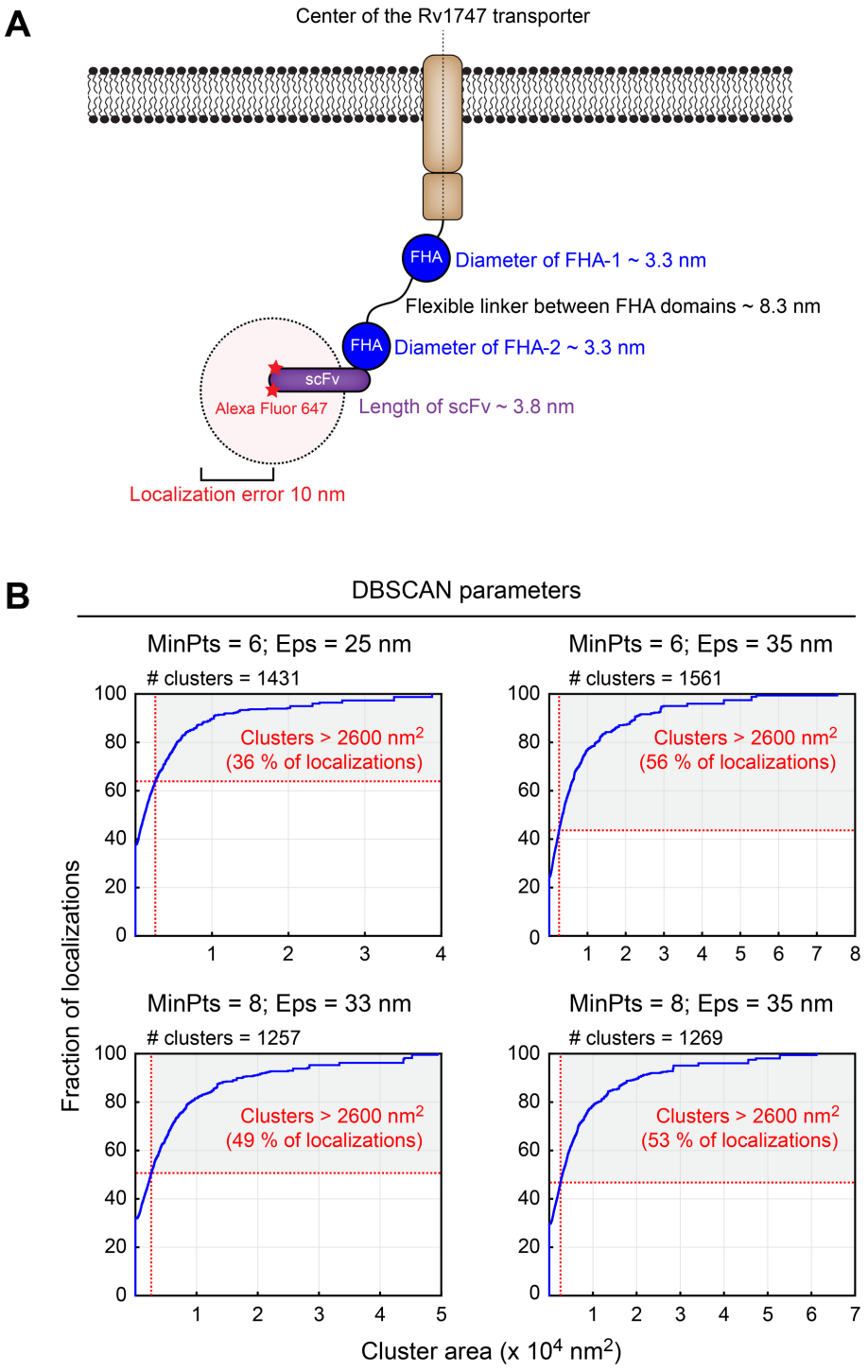


**Fig. S15. DBSCAN parameter choice does not change the outcome of cluster quantification.** (*A*) Schematic representation of Rv1747. As explained in the Supplementary Methods, the dimensions of individual FHA domains, linker, AF647-labeled scFv and a SMLM localization

error are included in the calculation to estimate the maximal length (~ 28.7 nm) and area (~ 2600 $nm^2$) occupied by a single molecule. (*B*) Distribution functions showing the cumulative fraction of all anti-Rv1747 AF647-scFv localizations from 45 *Mtb* cells identified as clusters using a range of DBSCAN parameters. These parameter are the minimum number (MinPts) of localizations within a distance cut-off (Eps) of each other used to define a cluster. The y-intercept is the fraction of non-clustered localizations (i.e. localizations not belonging to any cluster detected by DBSCAN). The vertical dashed lines are at a cluster area of 2600 $nm^2$, the maximal area generously estimated to be occupied by a single Rv1747 molecule. The choice of DBSCAN parameters does not change the conclusion that approximately half of the localizations are organized into clusters with areas greater than this limit.

**Supplemental Movies**

**Supplemental Movie S1.** Movie of the coalescence of two msfGFP-Rv1747$^{1-310}$ foci in *S. cerevisiae*.

**Supplemental Movie S2.** *M. smegmatis* expressing mEos2 (*left column*), mEos2-Rv1747 (*middle*) and mEos2-Rv1747$^{1-310}$ (*right*) were settled on poly-L-lysine coated coverslips and imaged for 10 seconds at 33 frames per second in TIRF. *Upper row* shows the raw images and *lower row* depicts the binary images of particles/foci above the detection criteria of the Icy Bioimaging software. mEos2 alone is uniformly distributed (*left*), while the regulatory module forms foci that predominantly persist during recording *(right*). Foci formed by full-length Rv1747 assemble and disassemble during imaging (*middle*). Scale bar = 5 μm.

**Supplemental Movie S3.** A 3D visualization of Rv1747-specific AF647-scFv single molecule localizations rendered using ViSP software. The localizations are color-coded based on density, ranging from dark red (low) to yellow (high). The grid size is 500 nm.

**References for SI Citations**


1. Wilkins MR, et al. (1999) Protein identification and analysis tools in the ExPASy server. *Methods Mol Biol* 112:531-552.
2. Foster LJ, De Hoog CL, Mann M (2003) Unbiased quantitative proteomics of lipid rafts reveals high specificity for signaling factors. *Proc Natl Acad Sci U S A* 100:5813-5818.
3. Wu JQ, McCormick CD, Pollard TD (2008) Chapter 9: Counting proteins in living cells by quantitative fluorescence microscopy with internal standards. *Methods Cell Biol* 89:253-273.
4. Banjade S, Rosen MK (2014) Phase transitions of multivalent proteins can promote clustering of membrane receptors. *Elife* 3:e04123.
5. Huang L-K, Wang M-JJ (1995) Image thresholding by minimizing the measures of fuzziness. *Pattern Recognition* 28:41-51.
6. Pedelacq JD, Cabantous S, Tran T, Terwilliger TC, Waldo GS (2006) Engineering and characterization of a superfolder green fluorescent protein. *Nat Biotechnol* 24:79-88.
7. Newton GL, et al. (2003) The glycosyltransferase gene encoding the enzyme catalyzing the first step of mycothiol biosynthesis (MshA). *J Bacteriol* 185:3476-3479.
8. McKinney SA, Murphy CS, Hazelwood KL, Davidson MW, Looger LL (2009) A bright and photostable photoconvertible fluorescent protein. *Nat Methods* 6:131-133.
9. de Chaumont F, et al. (2012) Icy: an open bioimage informatics platform for extended reproducible research. *Nat Methods* 9:690-696.
10. Bach H, et al. (2001) *Escherichia coli* maltose-binding protein as a molecular chaperone for recombinant intracellular cytoplasmic single-chain antibodies. *J Mol Biol* 312:79-93.

11. Glass LN, et al. (2017) *Mycobacterium tuberculosis* universal stress protein Rv2623 interacts with the putative ATP binding cassette (ABC) transporter Rv1747 to regulate mycobacterial growth. *PLoS Pathog* 13:e1006515.

12. Kamariza M, et al. (2018) Rapid detection of *Mycobacterium tuberculosis* in sputum with a solvatochromic trehalose probe. *Sci Transl Med* 10.

13. Cimino M, Alamo L, Salazar L (2006) Permeabilization of the mycobacterial envelope for protein cytolocalization studies by immunofluorescence microscopy. *BMC Microbiol* 6:35.

14. Tafteh R, et al. (2016) Real-time 3D stabilization of a super-resolution microscope using an electrically tunable lens. *Opt Express* 24:22959-22970.

15. Tafteh R, Scriven DR, Moore ED, Chou KC (2016) Single molecule localization deep within thick cells; a novel super-resolution microscope. *J Biophotonics* 9:155-160.

16. Dempsey GT, Vaughan JC, Chen KH, Bates M, Zhuang X (2011) Evaluation of fluorophores for optimal performance in localization-based super-resolution imaging. *Nat Methods* 8:1027-1036.

17. Ester M, Kriegel H-P, Sander J, Xu X (1996) A density-based algorithm for discovering clusters in large spatial databases with noise. *Proceedings of the Second International Conference on Knowledge Discovery and Data Mining (KDD-96); Simoudis, E., Han, J. and Fayyad, U.M., eds.*:226–231.

18. Marsh JA, Forman-Kay JD (2010) Sequence determinants of compaction in intrinsically disordered proteins. *Biophys J* 98:2383-2390.

19. Moglich A, Joder K, Kiefhaber T (2006) End-to-end distance distributions and intrachain diffusion constants in unfolded polypeptide chains indicate intramolecular hydrogen bond formation. *Proc Natl Acad Sci U S A* 103:12394-12399.

20. Spivey VL, et al. (2011) Forkhead-associated (FHA) domain containing ABC transporter Rv1747 is positively regulated by Ser/Thr phosphorylation in *Mycobacterium tuberculosis*. *J Biol Chem* 286:26198-26209.

21. Heinkel F, et al. (2018) Biophysical characterization of the tandem FHA domain regulatory module from the *Mycobacterium tuberculosis* ABC Transporter Rv1747. *Structure* 26:972-986.